Proof of Concept of Model-based Cardiovascular Prediction

Call identifier: FP7-ICT-2013-10 - **Grant agreement no**: 611232

Thematic Priority: ICT-2013.5.2: Virtual Physiological Human

Deliverable 4.3

Implementation of full mechanics parametrization method

Due date of delivery: March 31st, 2015

Actual submission date: November 20th, 2015

Start of the project: 1st October 2013
Ending Date: 30th September 2016

Partner responsible for this deliverable: MUG

Version: 0.2

Dissemination Level: Public

Document Classification

Title	Implementation of full mechanics parametrization method
Deliverable	4.3
Reporting Period	October 2013 – March 2015
Authors	MUG
Work Package	WP4 – Electro-mechanical model of the heart
Security	PU
Nature	Report
Keyword(s)	Software, finite element, parametrization

Document History

Name	**Remark**	**Version**	**Date**
Gernot Plank	First draft	0.1	26th March 2015
Gernot Plank	Updated version	0.2	9th November 2015

List of Contributors

Name	**Affiliation**
Gernot Plank	MUG
Christoph Augustin	MUG
Anton Prassl	MUG
Andrew Crozier	MUG
Aurel Neic	MUG

List of reviewers

Name	**Affiliation**
Edwin Morley-Fletcher	LYNKEUS

Abbreviations

FE	**Finite Element**
CARP	**Cardiac Arrhythmia Research Package**
LDRB	**Laplace Dirichlet Rule Based Method**
LV	**Left Ventricle**
RV	**Right Ventricle**
LA	**Left Atrium**
RA	**Right Atrium**
PV	**Pulmonary Veins**
TGV	**Total Genearlized Variation**
AV	**Atrio-ventricular node**
PS	**Purkinje system**
PVJ	**Purkinje-ventricular junction**
EDPVR	**Enddiastolic Pressure Volume Relation**
ESPVR	**Endsystolic Pressure Volume Relation**
IVC	**Isovolumetric Contraction**
IVR	**Isovolumetric Relaxation**
ED	**Enddiastole**
EDP	**Enddiastolic Pressure**
EDV	**Enddiastolic Volume**
WP	**Work Package**

Contents

Executive Summary

The main objective of D4.3 is the development of parametrization and data assimilation strategies for patient specific modelling of ventricular mechanics. A mechanical model of ventricular deformation consists of four main components, an anatomical finite element model representing the geometry of the heart, a constitutive model describing the passive mechanical properties of ventricular tissue, an active stress model, which drives contraction and relaxation of the ventricles, and a lumped haemodynamic model of the cardiovascular system to serve as a pressure-volume (PV) boundary condition during the ejection phase. All model components require patient-specific parameterization, which is based on haemodynamic pressure-volume data measured clinically prior to treatment. The model components, their parametrization and the relative role they play over a full cardiac cycle within a PV loop are summarized in Figure 1.

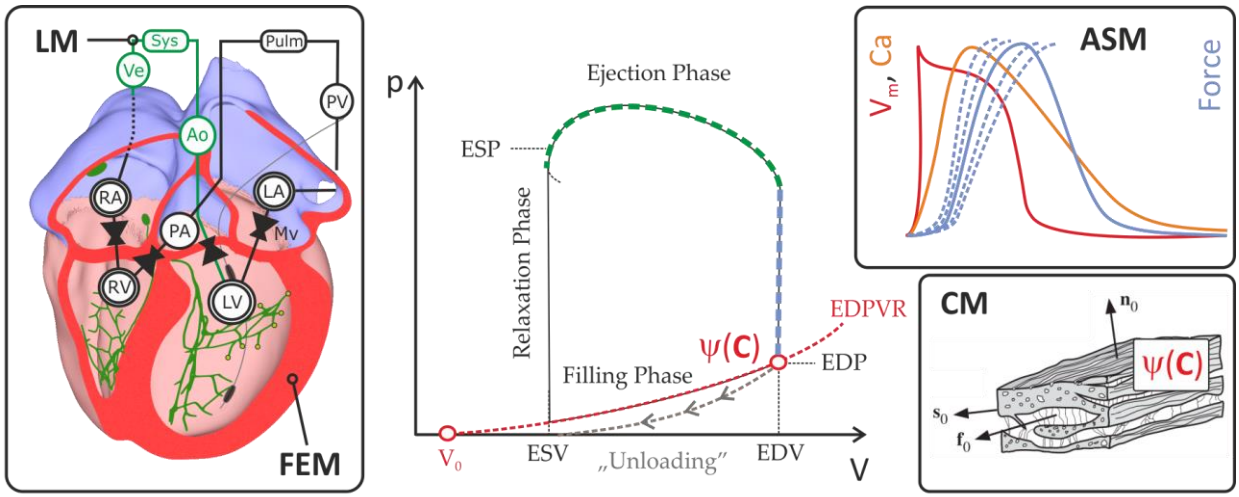

Figure 1 Mechanics model components and parametrization based on haemodynamic pressure-volume data. Lower right panel: Passive mechanical properties of the ventricular muscle are described by a strain-energy function ψ, referred to as constitutive model (CM). Properties of ψ govern the passive P-V behaviour during diastole and thus define EDPVR (red dashed line). Right upper panel: The active stress model (ASM) governs force of contraction during IVC and ejection phase, and relaxation during the IVR. Left panel: Anatomy is represented as a FEM model coupled to a lumped model of the cardiovascular system. This model governs the ejection phase of the pressure volume loop (green-dashed line).

Introduction

The focus of this work is on the development of parametrization and data assimilation strategies for achieving a close match between clinically measured PV loops and those predicted by the computational model of a given patient. This necessitates the implementation of four parameterization steps

1. An algorithm will be implemented which derives the unloaded reference configuration from the end-diastolic geometry.
2. Passive mechanical properties are fitted to match a patient's end-diastolic pressure-volume relations (EDPVR) using a single pressure-volume pair acquired at end diastole. EDPVR is assumed to follow an exponential relation based on empirical data [Klotz 2007]
3. Active contractile model parameters are fitted to patient data by comparing simulated pressure traces during the isovolumetric contraction (IVC) phase with catheter pressures measured in the patient.
4. Pressure and volume in the ventricular cavities during ejection is dictated by the force generated by the ventricles as well as by resistance and compliance of the attached cardiovascular system. Both factors govern afterload, that is, the ventricular wall stresses during the ejection phase. Lumped models of the cardiovascular system are used as a constraint. Parameters in the lumped model need to be identified to match the observed pressure and volume traces in a given patient.
5. Alternative strategies for dealing with mechanical boundary conditions were implemented to improve the match between model prediction and imaging data, and to better constrain the problem to achieve robust convergenceof elasticity solvers.

Computing a stress-free reference configuation

The cardiac anatomy represented in a computer model is typically discretized based on a 3D segmentation of a tomographic image stack acquired at end-diastole (ED). In its enddiastolic state the endocardium is subjected to an end-diastolic pressure (EDP) of around 10 mmHg. To quantify stresses in the myocardium

the geometry under zero stress, i.e. *the stress free reference configuration* has to be derived, since the zero pressure unstressed geometry in general cannot be measured *in-vivo*. Applying EDP to a geometric model based on ED geometry would further inflate the ventricles, thus leading to an inconsistent state, which cannot be matched with a given patients physiology. This inconsisteny would bias the underlying passive end-diastolic pressure volume relationship.

Various approaches for this specific problem have been proposed in the literature, mostly for vascular mechanics applications [Bols], which is geometrically simpler compared to modelling a ventricle and attached Aorta in a combined model, but also for biventricular models [Rajagopol 2008, Krishnamoorthy 2013]. Finding the stress free reference configuration can be posed as an inverse problem of finding the configuration $\Omega_{?}(\mathbf{x}_0,0)$ from $\Omega_{??}(\mathbf{x}_{ED}, 0)$ such that $\Omega_{?}(\mathbf{x}_0, 0)$ maps onto $\Omega_{??}(\mathbf{x}_{ED}, p_{ED})$ when inflating the stress free reference configuration up to the end-diastolic configuration.

As an unloading algorithm the backward displacement method due to Bols was implemented, as this method is particularly simple to implement within a FE modeling framework. The method is identical to the method reported by Krishnamoorthy et al for a biventricular model [Krishnamoorthy 2013]. The basic procedure is as follows: In a first step the image-derived end-diastolic model is assumed to be in an unloaded reference state and inflated up to the EDP. An approximation to the inverse of the resulting deformation is then applied to the end-diastolic mesh by subtracting the displacement from the end-diastolic configuration, thereby yielding a new approximation of the unloaded reference geometry. This procedure is applied repeatedly until convergence is achieved. For the sake of illustration the underlying concept is illustrated in a geometrically simplified left ventricular slice model in Figure 2. The implemented algorithmic steps are summarized in Figure 3.

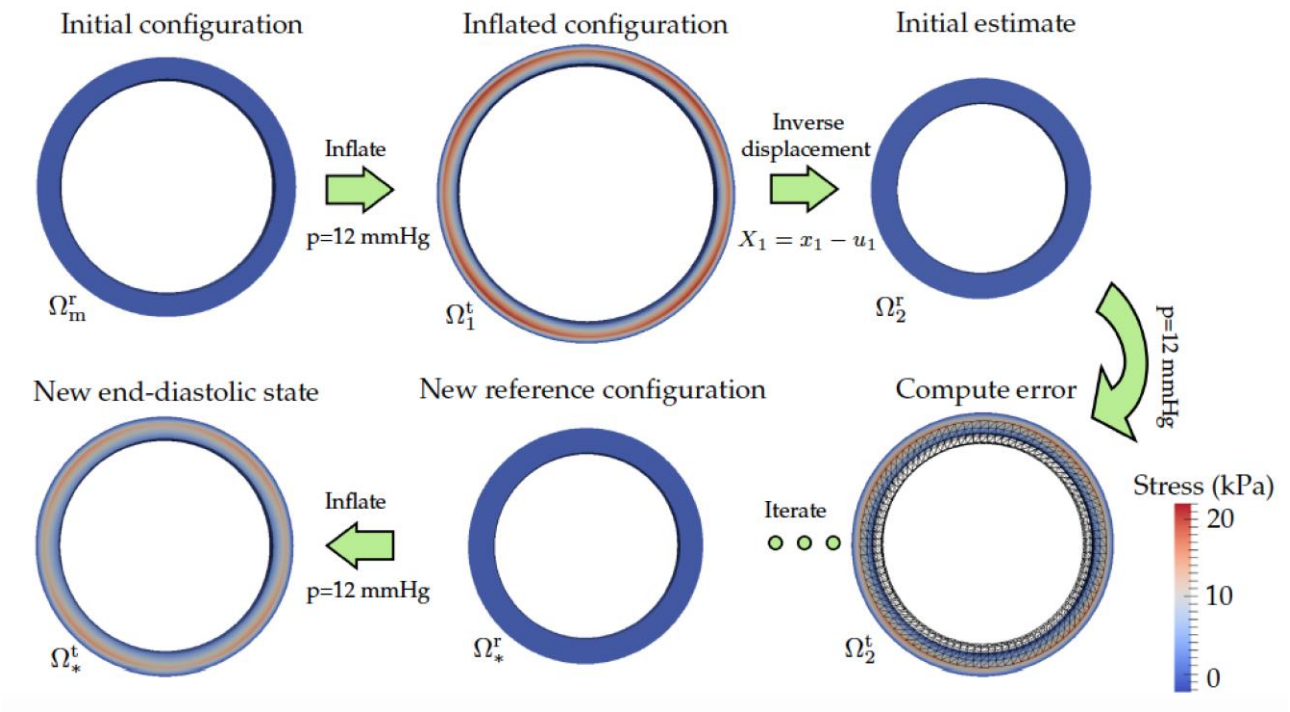

Figure 2: Basic principle of a backward displacement method. As an initial configuration the imaged enddiastolic geometry is used which is inflated up to the measured EDP. Subsequently, the inverse displacement is applied to the EDP configuration, yielding now an initial estimate of the unloaded stress free configuration. This configuration is then inflated again up to the EDP. An error can be computed then as the difference between this configuration and the known correct EDP geometry.

Algorithm 1 Backward displacement method

Require: Measured end-diastolic state $\Omega^{\mathrm{r}}_{\mathrm{m}} := \Omega(\boldsymbol{x}_{\mathrm{m}}, 0)$ and measured pressure load p_{m}

$i = 0$

Set initial stress-free configuration $\Omega^{\mathrm{r}}_0 := \Omega(\boldsymbol{X}_0, 0)$ with coordinates $\boldsymbol{X}_0 = \boldsymbol{x}_{\mathrm{m}}$

while $r^i_{\max} \geq \varepsilon$ **do**

  $i = i + 1$

  $\Omega^t_i := \Omega(\boldsymbol{x}_i, \boldsymbol{\sigma}_i) = \mathcal{I}_i(\Omega^{\mathrm{r}}_i, p_{\mathrm{m}})$ ▷ Inflate using measured pressure load p_{m}

  $\boldsymbol{U}_i = \boldsymbol{x}_i - \boldsymbol{X}_i$

  $\boldsymbol{X}_{i+1} = \boldsymbol{x}_{\mathrm{m}} - \boldsymbol{U}_i$ ▷ Inverse displacement

  $\Omega^{\mathrm{r}}_{i+1} := \Omega(\boldsymbol{X}_{i+1}, 0)$

  $r^i_{\max} = \mathrm{ERR}(\Omega^{\mathrm{r}}_{\mathrm{m}}, \Omega^t_i)$ ▷ Compute error

end while

Zero-pressure reference geometry $\Omega^{\mathrm{r}}_* := \Omega(\boldsymbol{X}_*, 0)$ with coordinates $\boldsymbol{X}_* = \boldsymbol{X}_i$

In vivo stress tensor $\boldsymbol{\sigma}_* = \boldsymbol{\sigma}_i$

New end-diastolic geometry $\Omega^t_* := \Omega(\boldsymbol{x}_*, \boldsymbol{\sigma}_*)$

Figure 3: Algorithmic pseudo-code of backward displacement method.

The application of the method is shown in Figure 4, using the geometry of patient dataset B0305-28 (Figure 4, right panels). Mathematically, while it is not guarantueed for a backward displacement method to converge, the residual error either measured as the norm of nodal distances or the difference in volumes between initial geometry and pre-stressed geometry after unloading and re-inflation, is continuously decreased by the implemented algorithm (Figure 4, left panel).

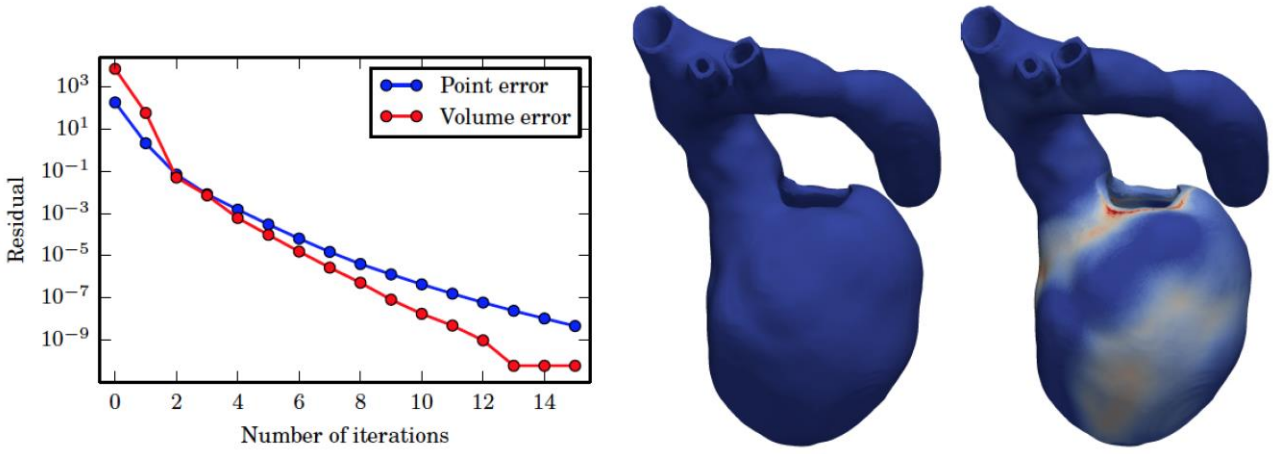

Figure 4: Unloading of a LV geometry with attached Aorta. Left panel shows the residual errors as a function of the number of iterations of the backward displacement loop. Residual errors were computed between initial geometry and the pre-stressed geometry after unloading and re-inflation up to EDP. The residuals were measured as the norm of nodal distances or the difference in volumes between the geometries. Middle panel: LV model in unloaded stress-free reference configuation. Right panel: LV model in end-diastolic configuration after inflation to EDP of the unloaded configuration. Colors encode stress distribution.

Fitting passive mechanical properties

After unloading and re-inflation, the model matches geometry and pressure at ED. Conversely, the stress-free reference state and ED pressure-volume relation (EDPVR) will depend on the passive material properties of the myocardium. EDPVR data from the clinic is often limited, so we instead fit to the generic Klotz relation and EDPVR [Klotz 2007].

Klotz et al. determined empirically that the stress-free volume V_0 of the left ventricle could be determined by the relation

$$V_0 = V_m(0.6 - 0.006P_m)$$

where (V_m, P_m) is a measured volume-pressure pair at ED. They also demonstrated that the EDPVR could be approximated by the power law

$$P = \alpha V^{\beta}$$

where

$$\alpha = \frac{30}{V_m^{\beta}} \qquad \beta = \frac{\log\left(\frac{P_m}{30}\right)}{\log\left(\frac{V_m}{V_{30}}\right)}$$

and V_{30}, the volume at a pressure of 30 mmHg, is given by

$$V_{30} = V_0 + \frac{V - V_0}{\left(\frac{P_m}{A_n}\right)^{1/B_n}}$$

To avoid a singularity in the above equations, α and β are given as follows when $P_m \geq 22$ mmHg

$$\alpha = \frac{P_m}{V_m^{\beta}} \qquad \beta = \frac{\log\left(\frac{P_m}{15}\right)}{\log\left(\frac{V_m}{V_{15}}\right)}$$

and V_{15}, the volume at a pressure of 15 mmHg, is given by

$$V_{15} = 0.8(V_{30} - V_0) + V_0$$

The constants A_n and B_n were determined empirically as 27.78 and 2.76 respectively. The volume units are ml and pressure units are mmHg. With the above relations, it is possible to estimate the stress-free volume and EDPVR for a patient, given their ED volume and pressure.

Fitting of the passive material parameters is then done by matching the computed stress-free LV cavity volume and EDPVR with those of the Klotz relation. For each trial parameter set, the unloading algorithm described above is used to compute the stress-free reference state, then a simulation of passive inflation back up to the end diastolic pressure is performed. This is performed for a number of trial parameter sets, with the one that best matches the Klotz EDPVR and stress-free volume selected as the fitted parameter space.

The example below in Figure 5 shows the fitting of a passive material model with an exponential strain-energy function to the Klotz relation. First, the pressure and volume at end diastole are used to compute

the reference volume V_0 and EDPVR, then a parameter sweep is run over the linear and exponential parameters of the model. The best matching model is taken as the fitted solution.

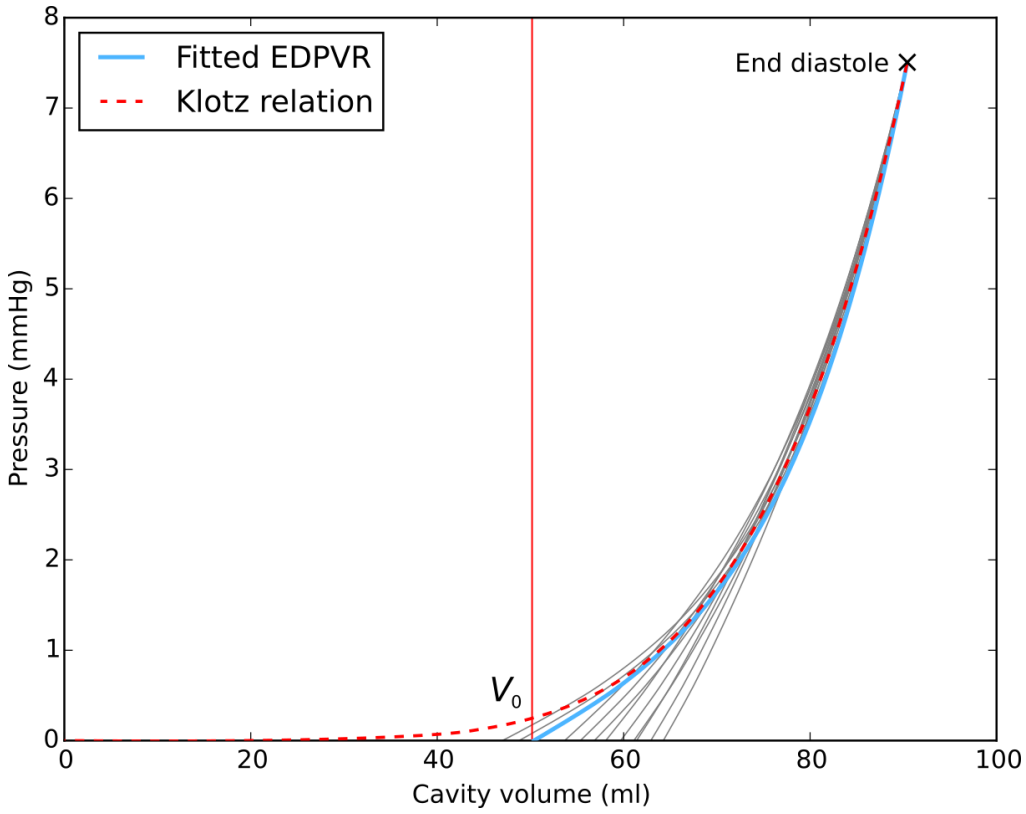

Figure 5 Klotz end-diastolic pressure-volume relation (EDPVR) (red dashed) and fitted EDPVR (blue) from a parameter sweep (grey). The fitted parameters are those that best predict both the stress-free volume V_0 and the Klotz relation.

Fitting active force generation

Active contractile model parameters have to be fitted to patient data by comparing simulated pressure traces during the isovolumetric contraction (IVC) phase with catheter pressures measured in the LV of a patient. The choice of the active stress model and the fitting procedure were based on finding a balanced trade-off between physiological detail, cost of simulation and identifiability of parameters. Finding this trade-off was guided by the main objective of approximating a given patient's heart beat as closely as possible in terms of motion of, and displacements and strains in the LV. For this sake a phenomenological contractile model was used in which two parameters, the maximum contractility, S_{peak}, and the time constant governing contraction, τ_c, relate to the two clinical key parameters of interest, namely peak pressure, p_{max} and the maximum rate of rise, dp/dt_{max}, in an intuitive manner. The exponential contractile model is given as

$$\sigma = S_{\text{peak}}\left(1 + e^{t'/\tau_c}\right)^{-1}\left(1 + e^{(t'-t_d)/\tau_r}\right)^{-1}$$

where $t' = t - t_{EMD}$ is the activation time minus the electromechanical delay (EMD), t_d is the duration of active contraction and τ_r is the time constant of relaxation. An example stress transient generated by this model is shown in Figure 6, along with an illustration of the effect of the τ_c and τ_r time constants.

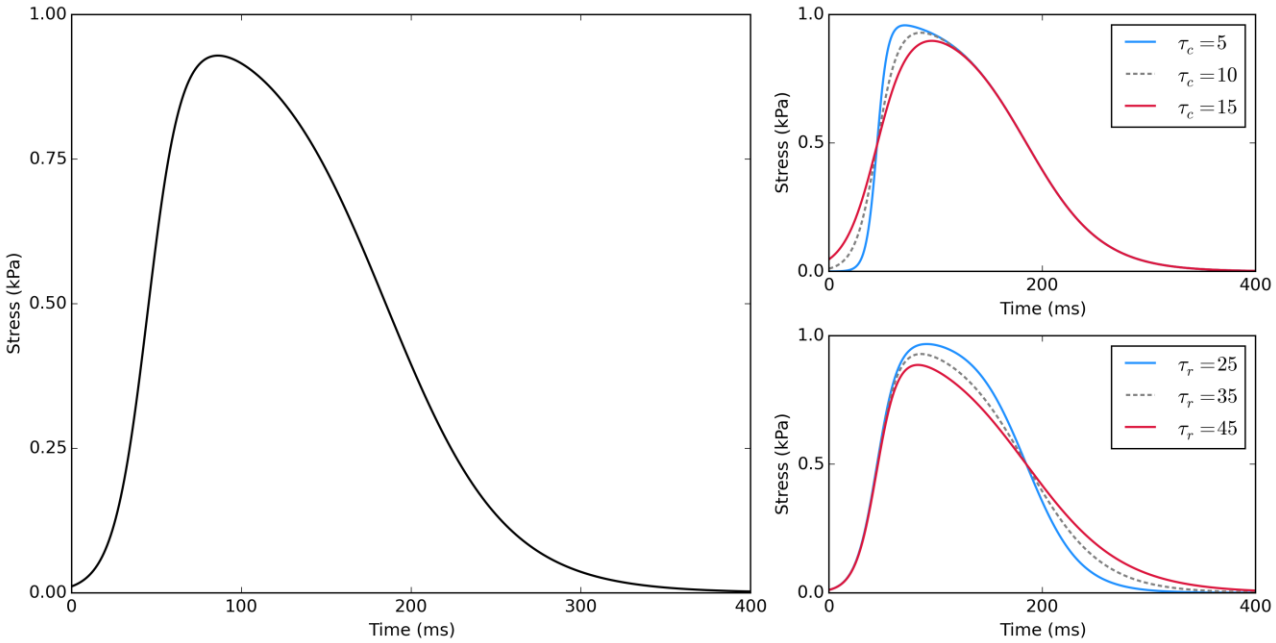

Figure 6 Myofibre stress over time according to the fixed stress model described above. The left panel shows the time evolution of the stress with S_{peak}=1kPa, τ_c=10ms, τ_r=35ms and t_d=140ms. On the right the effect of changing the τ_c (above) and τ_r (below) parameters is illustrated. Here blue indicates a shorter time constant and red a longer time constant.

The time constant governing relaxation has not been considered for fitting as the physiological details of the LV relaxation and filling are of lesser relevance with respect to our main objectives.

Since the chosen active stress model does not account for length dependence of active force generation, i.e. the cellular Starling mechanisms, the fitting of p_{max} and dp/dt_{max} can be performed by adjusting S_{peak} and τ_c individually with limited cross-talk between the two procedures. Results of a parameter sweep over S_{peak} for a prescribed τ_c of 10 ms are summarized in Figure 7. The result of a combined sweep The result of a combined sweep over S_{peak} (range from 80 kPa to 200 kPa) and τ_c (range from 10 to 70 ms) is given in Figure 8. Using these summary plots an appropriate choice of S_{peak} and τ_c can be made using the clinically observed parameters p_{max} and dp/dt_{max} as input.

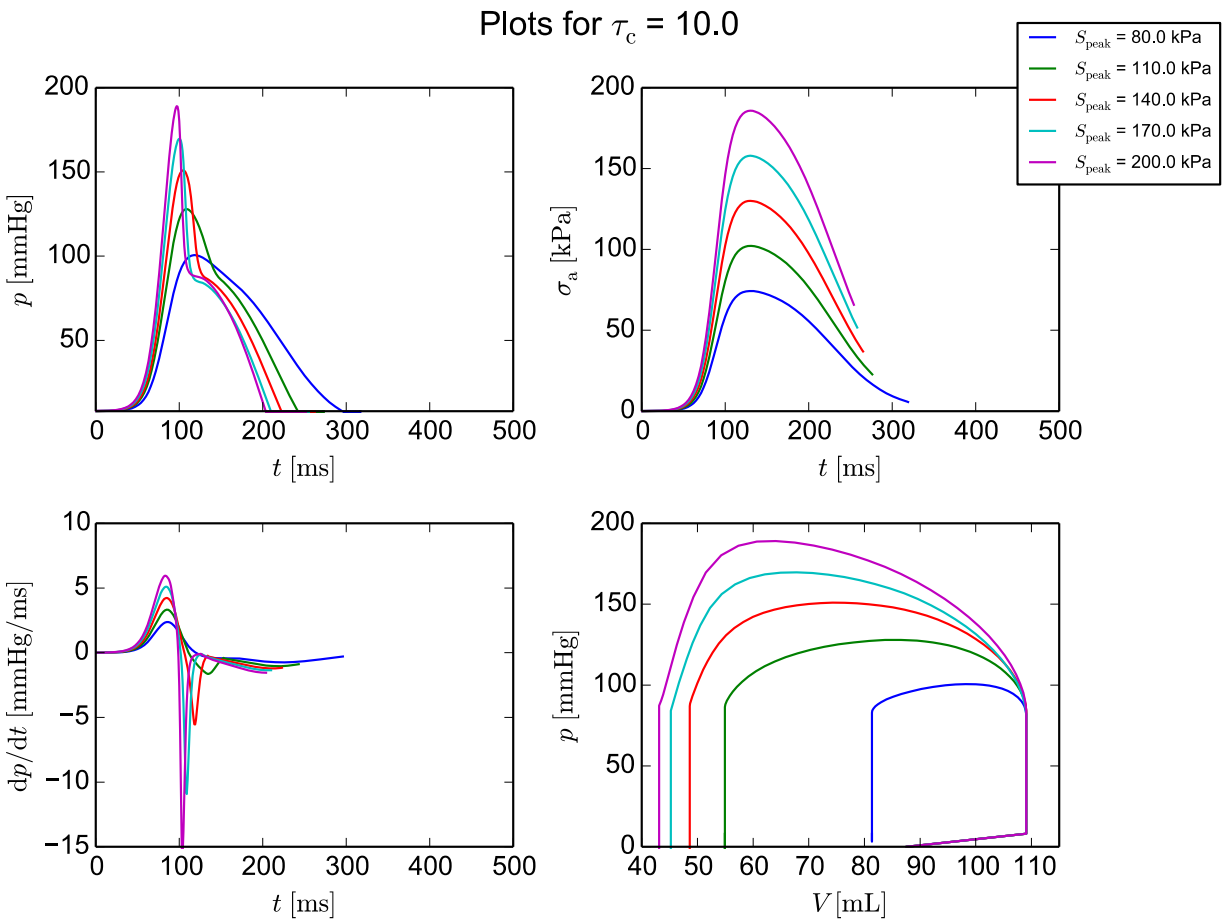

Figure 7 Results of parameter sweep over contractility S_{peak} for a given time constant of contraction, τ_c, of 10 ms.

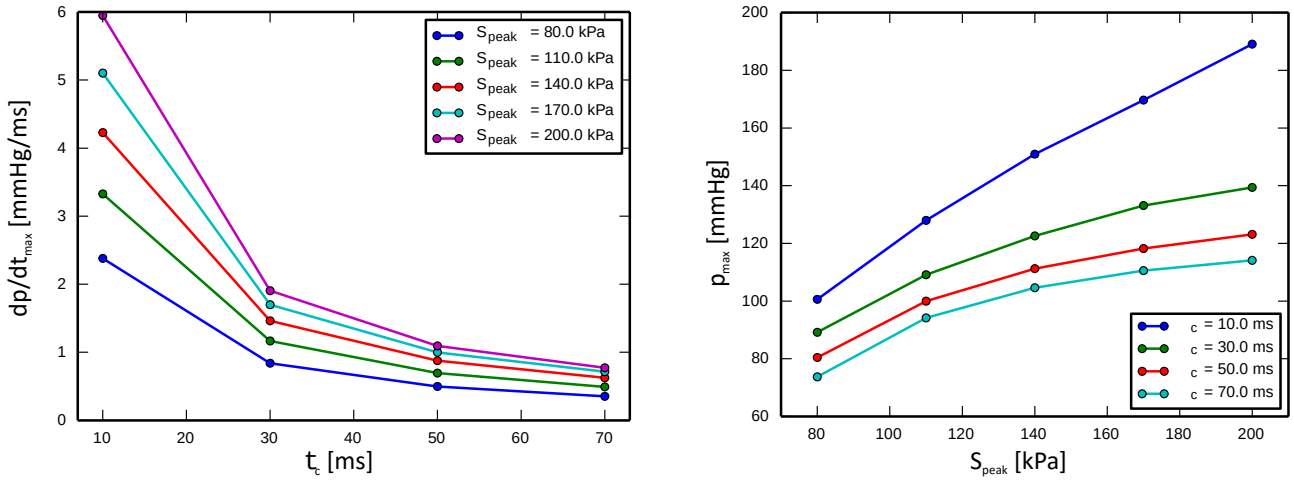

Figure 8 Maximum rate of rise of LV pressure and peak LV pressure as a function of peak contractility and the time constant governing the rate of rise of contraction.

Fitting cardiovascular system parameters

Pressure and volume in the ventricular cavities during ejection is dictated by the force generated by the ventricles as well as by resistance and compliance of the attached cardiovascular or pulmonary system. Both factors govern afterload, that is, the ventricular wall stresses during the ejection phase. Lumped models of the cardiovascular system are used as a constraint. While pressure and volume flow in all four chambers are linked, for modelling the ejection of the left ventricle, only resistance and compliance of the cardiovascular system matter. The most popular lumped afterload model for such applications is the 3 element Windkessel model due to Westerhof [Westerhof 1971]. The Parameters of the lumped 3 element Windkessel model need to be identified to match the observed pressure and volume traces in a given patient. In the following we describe the methodological underpinnings of the implemented approach.

Three element Windkessel Model

Lumped parameter models of the circulation are commonly used when modelling cardiac electromechanics, as they provide a readily parameterisable and computationally inexpensive representation of blood flow out of the heart. Some groups [Constantino 2012, Gurev 2011, Hu 2013 Hu 2014, Kerckhoffs 2007, Kerckhoffs 2009, Krishnamurthy 2013] use the closed loop circulation model introduced by Kerckhoffs et al. [6], in which blood flow returns to the heart after passing through a simplified representation of the vasculature. Others use 3 [Aguado-Sierra 2011, Niederer & Lamata 2012, Niederer 2012, Niederer 2011, Sugiura 2012] or 4 [Marchesseau 2013, Sermesant 2012] element Windkessel models. The standard 3 element model can be illustrated as its analogous electrical circuit, as shown in Figure 9.

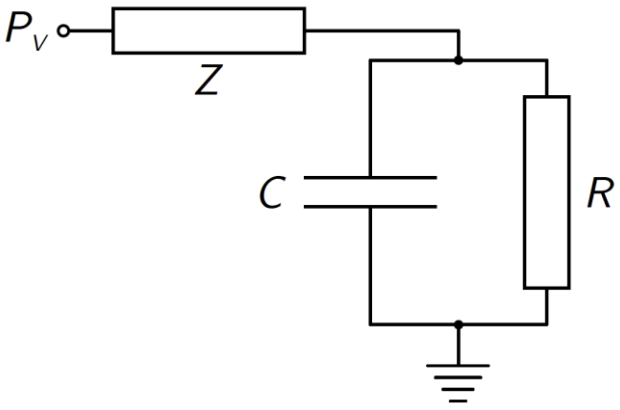

Figure 9 Circuit diagram of the 3 element Windkessel model of arterial resistance to blood flow. Ventricular pressure P_V is linked to a zero pressure sink through a resistance Z in series with a parallel resistance R and capacitance C.

In such an electrical analogy, pressure P_V corresponds to electrical potential and flow rate U corresponds to current. Applying standard laws of electrical circuits, one may derive the following differential equation to model the evolution of the system

$$\frac{dU}{dt} = \frac{P}{ZRC} + \frac{1}{Z}\frac{dP}{dt} - \left(\frac{1}{ZC} + \frac{1}{RC}\right)U \quad (1)$$

where Z is the aortic resistance, and R and C are the resistance and compliance of the peripheral arterial circulation respectively. The four element Windkessel model [Stergiopulos 1999] includes inertial effects by adding an inductor in parallel to the first resistor (Z in Figure 9).

Closed loop models provide the possibility of analysis of beat to beat haemodynamic effects, however the computational cost of running multiple beat simulations can be prohibitive. For this reason, and due to the limited data available to characterise the extra parameter in the 4 element model, we opted for using the 3 element Windkessel model in our cardiac electromechanics framework.

Parameter Fitting

As the Windkessel model relates only pressure and volume in the ventricle, it was possible for us to fit it directly to PV data, without coupling to the model of large deformation mechanics. Fitting Windkessel model parameters is computationally inexpensive, however care had to be taken to ensure physiological parameters were chosen, as described below.

Combining the Windkessel model ODE above with the following linking ventricular cavity volume *V* and blood flow out of the ventricle *U*

$$\frac{dV}{dt} = -U \qquad (2)$$

we can solve this system of equations using the pressure transient during the ejection phase as an input to calculate the corresponding ventricular volume over time. Note that Eq. 2 has a negative sign as a positive ow out of the ventricle U implies a decreasing ventricular volume V. These equations are solved numerically using the ODE integrator from the SciPy scientic Python library. Model parameters are then fitted by matching the volume trace calculated by this method with the clinically recorded volume trace. Using a naive cost function for parameter fitting, consisting of the l2 norm of the dierences between the simulated and clinical volume transients at a set of sample times, do not produce reasonable results. As shown in the example in Figure 10, the Windkessel model parameter values fitted by this method predict volume transients which closely match the clinical data, but do not predict a reversal of flow direction at the end of ejection. We do not wish such a flow to occur in our model, but the reversal of flow direction is necessary to trigger the closure of the aortic or pulmonary valve and the subsequent change of phase to IVR in our full model of cardiac mechanics.

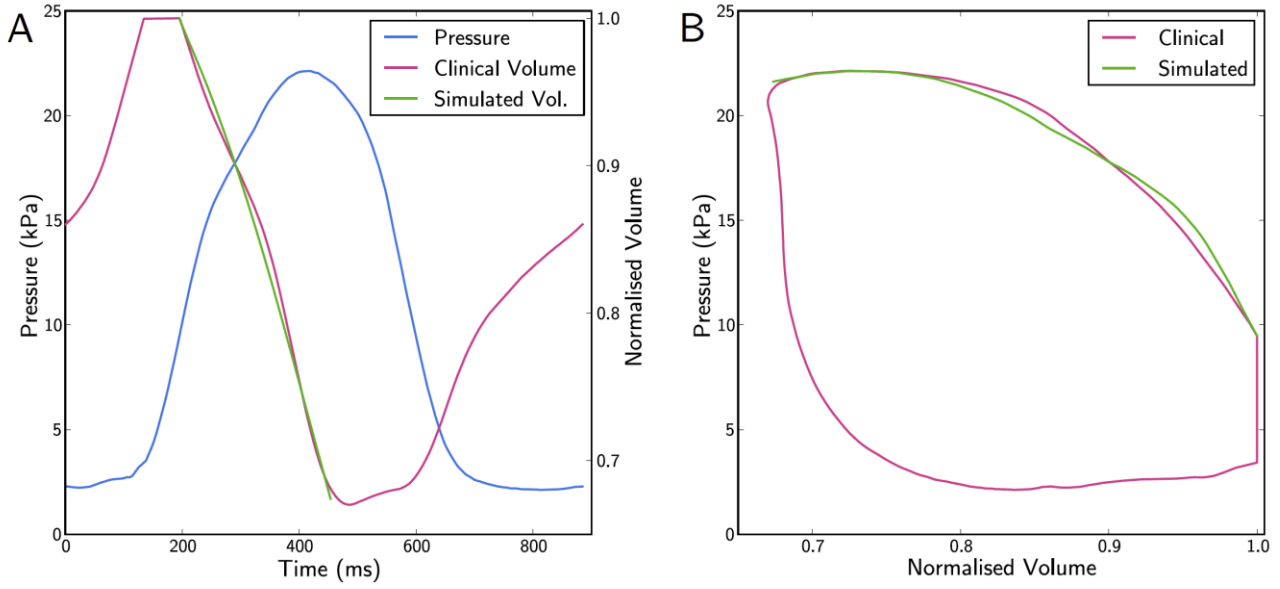

Figure 10 Example of a Windkessel model fitting attempt using a simple l2 norm cost function. As seen on the simulated volume trace (A) and PV loop (B), there is a close match between the simulated and clinical volume traces. However, the lack of predicted retrograde flow at the end of ejection undermines the model's utility.

The residual is therefore modied to include a constraint forcing retrograde flow at the end of ejection. The residual vector r, whose elements $\{r_i\}$ are the sampled differences between the simulation and clinical volume transients, is augmented by the fractional difference of the simulated ejection duration t_{Ej} and ejection fraction EF with that of the clinical data

$$\boldsymbol{r} = \left[r_1 \cdots r_n \; 2\frac{\Delta t_{Ej}}{t_{Ej}} \; 2\frac{\Delta EF}{EF}\right]^T \qquad (3)$$

The fractional differences and are scaled by a factor of 2 to increase their weighting with respect to the volume sample errors $\{r_i\}$. The cost function, including a penalty for no flow reversal is then

$$R = \begin{cases} \|r\| & \text{if flow reversal occurs} \\ 10^{10} & \text{otherwise} \end{cases}$$

An example of a model fitted using the augmented constraint can be seen in Figure 11. The Windkessel model parameters and the time of the start of ejection are fitted to the clinical volume trace with a combination of parameter sweeps and local refinement using the implementation of the downhill simplex algorithm in the SciPy scientific Python library. This combination of approaches is used as there are many local minima over the parameter space, and all tested optimisation algorithms converge to a result that is highly dependent on the initial guess. We therefore run a large set of optimisations from different initial guesses, which are chosen using a full factorial experimental design. Using this approach, Windkessel model parameters are fitted for the LV, taking around 15 minutes per case using a single core on a workstation computer.

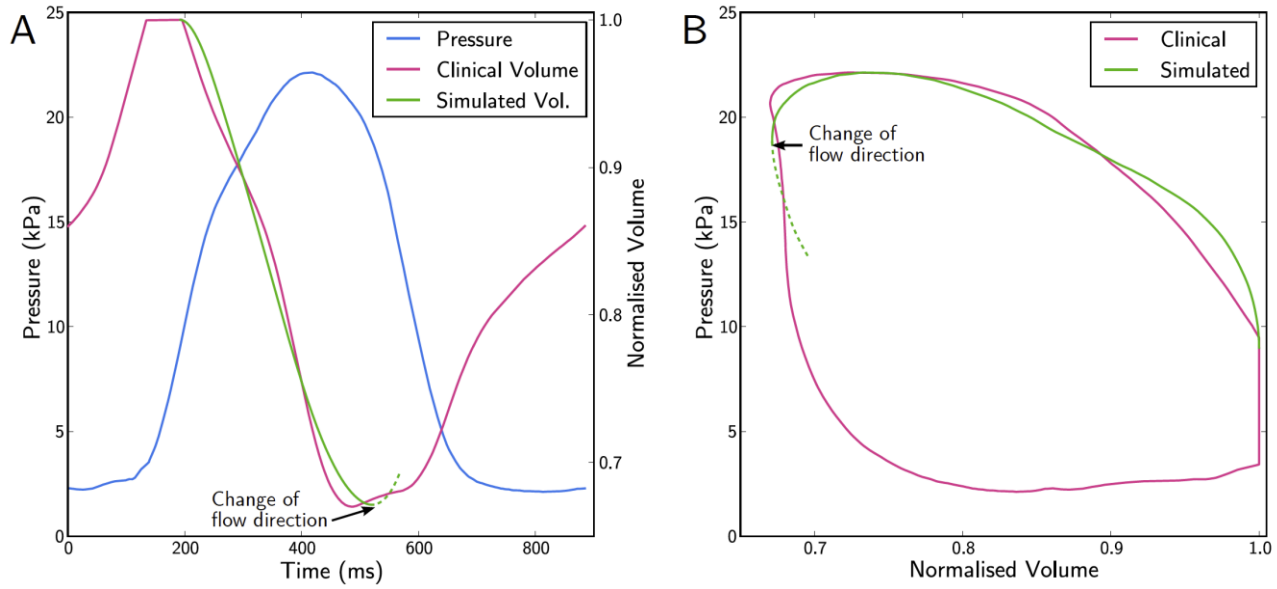

Figure 11 Example of a Windkessel model simulation with parameters itted using the improved cost function enforcing the prediction of retrograde flow at the end of ejection. As can be seen on the simulated volume trace (A) and PV loop (B), the model predicts the flow of blood back into the ventricle from the aorta, as indicated by the dashed line. This reverse flow is not seen in a real heart cycle, as the aortic valve closes to prevent retrograde flow, and the heart enters the IVR phase.

The above process has been applied successfully to patient B0305-28, with the fitted Windkessel predicted volume and PV loop shown below in Figure 12.

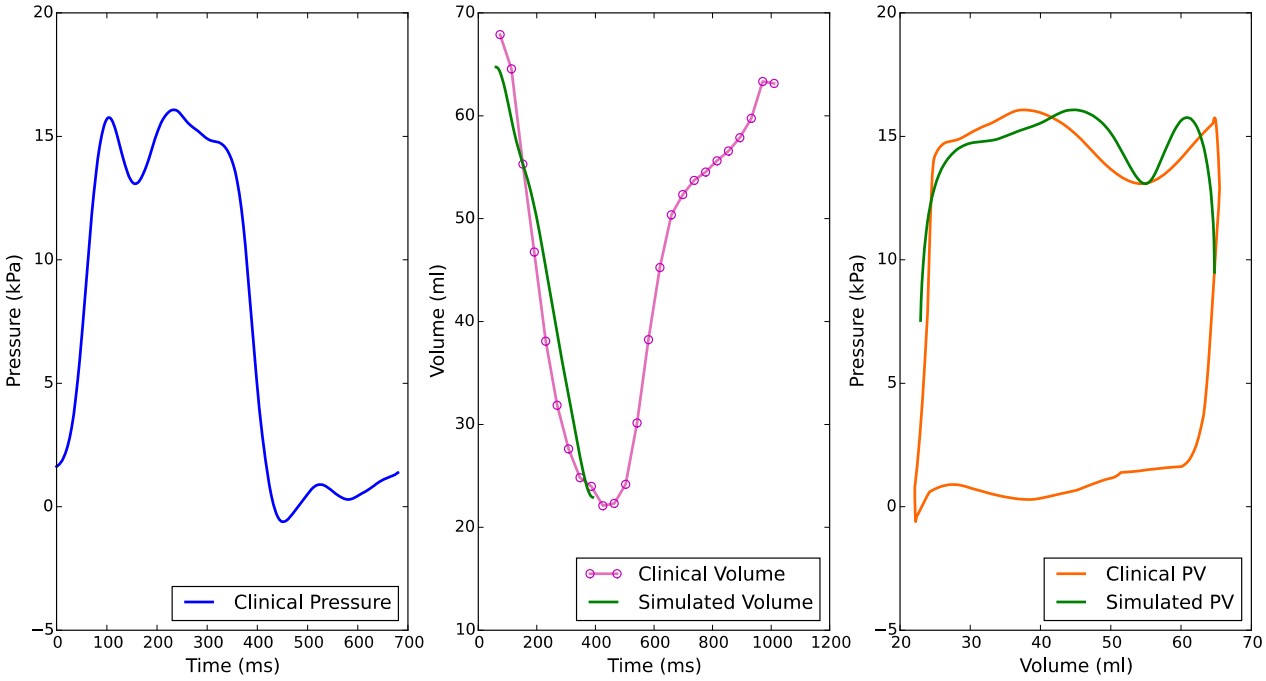

Figure 12 Fitted Windkessel model for patient B0305-28. The clinical pressure trace (left) was used as input to the Windkessel model to predict ventricular volume over time (middle, green). This was fitted to minimise error with the clinical volume trace (middle, magenta). The clinical PV loop and Windkessel-predicted PV relationship are shown on the right, in orange and green respectively.

Derivative-based Parameter Fitting Approach

Optimization methods such as a downhill simplex method are popular in the engineering communities, as they avoid the calculation of derivatives, making their implementation simpler. While these methods can be efficient, there are various drawbacks as well among which the most important ones are that convergence cannot be proven or guarantueed amd the speed of convergence might be slow. More elaborate derivative-based parameter identification approaches are likely to be more robust and efficient. As an alternative a derivative-based ODE constraint optimization method was implemented.

Optimization Problem

The fitting of the Windkessel parameters can be posed as an optimization problem

$$\min_{Z,R,C} \frac{1}{2}\int_0^T (U - U_m)^2 dt + \frac{\alpha}{2}(Z^2 + C^2 + R^2) \qquad (4)$$

$$s.t. \quad \frac{dU(t)}{dt} = \frac{P(t)}{ZRC} + \frac{1}{Z}\frac{dP(t)}{dt} - \left(\frac{1}{ZC} + \frac{1}{RC}\right)U(t) \qquad (5)$$

We call the reduced objective $j(Z,R,C)$ and its gradient $j(Z,R,C)$. For derivative-based optimization we provide the gradient g via Lagrange calculus. Therefore, an evaluation of j and g at the current iterate (Z,R,C) needs the following steps:

1. Solve the state equation (5) for U, compute j from (4)

2. Solve the adjoint equation for the adjoint state $q(t)$

$$\frac{dq(t)}{dt} = \left(\frac{1}{ZC} + \frac{1}{RC}\right) q(t) + U(t) - U_m(t), \quad q(T) = 0 \qquad (6)$$

3. Evaluate the reduced gradient g via computing the integrals

$$g = \begin{pmatrix} \alpha Z + \int_0^T q(t)\left[-\frac{1}{Z^2RC}P(t) - \frac{1}{Z^2}\frac{dP(t)}{dt} + \frac{1}{Z^2C}U(t)\right]dt \\ \alpha R + \int_0^T q(t)\left[-\frac{1}{ZR^2C}P(t) + \frac{1}{R^2C}U(t)\right]dt \\ \alpha C + \int_0^T q(t)\left[-\frac{1}{ZRC^2}P(t) + \left(\frac{1}{ZC^2} + \frac{1}{RC^2}\right)U(t)\right]dt \end{pmatrix} \qquad (7)$$

Discretization

The time grid is denoted by $0 = t_0 < \cdots < t_0 = T$. $P(t)$ is assumed to be given as piecewise linear function with values $P(t_i) = P_i$. Accordingly, dP/dt is piecewise constant. For consistent discrete derivatives, we apply the DG(0)-disretization, which corresponds to the implicit Euler. Therefore, both U and q are piecewise constant functions. The discrete state equation results as

$$\left(1 + \tau_i\left[\frac{1}{ZC} + \frac{1}{RC}\right]\right) U_i = U_{i-1} + \tau_i\left(\frac{P_i + P_{i-1}}{2ZRC} + \frac{1}{Z}\frac{P_i - P_{i-1}}{\tau_i}\right), \quad i = 1, \cdots, N \qquad (8)$$

with given initial value U_0 and time step size $\tau_i = t_i - t_{i-1}$. The objective is disretized accordingly as

$$\frac{1}{2}\sum_{i=1}^{N} \tau_i \, (U_i - U_{mi})^2 + \frac{\alpha}{2}(Z^2 + R^2 + C^2). \qquad (9)$$

The consistent discretization of the adjoint eqution is

$$\left(1 + \tau_i\left[\frac{1}{ZC} + \frac{1}{RC}\right]\right) q_i = q_{i-1} + \tau_i(U_i - U_{mi}), i = 1, \cdots, N \qquad (10)$$

with $q_{N+1} = 0$. The discrete reduced gradient results in

$$g = \begin{pmatrix} \alpha Z + \sum_{i=1}^{N} q_i\left[-\frac{1}{Z^2RC}\frac{P_i + P_{i-1}}{2} - \frac{1}{Z^2}\frac{P_i - P_{i-1}}{\tau_i} + \frac{1}{Z^2C}U_i\right]dt \\ \alpha R + \sum_{i=1}^{N} q_i\left[-\frac{1}{ZR^2C}\frac{P_i + P_{i-1}}{2} + \frac{1}{R^2C}U_i\right]dt \\ \alpha C + \sum_{i=1}^{N} q_i\left[-\frac{1}{ZRC^2}\frac{P_i + P_{i-1}}{2} + \left(\frac{1}{ZC^2} + \frac{1}{RC^2}\right)U_i\right]dt \end{pmatrix} \qquad (11)$$

Implementation

The implementation is done in Matlab. Both, the objective value j and its gradient g are implemented, as described above. For optimization we call *fmincon* using the *BFGS* variant. Pros and cons of the gradient-based optimization approach are currently being evaluated.

Mechanical boundary conditions

Physiological Background

The deformation of cardiac tissue is governed not only by the hyperelastic passive response of the myocardium and the active stresses generated during contraction, but also by external loads due to interaction with surrounding structures of the torso, in which the heart is embedded, such as the pericardium, lungs and large vessels. Mechanical boundary conditions therefore play a highly important role in cardiac pumping function, however they are particularly challenging to model in a physiologically correct fashion.

In most modeling studies, due to the mechanical complexity of how the heart is anchored within the torso, the inclusion of physiologically appropriate mechanical boundary conditions has not been addressed. Most studies applied non-physiological Dirichlet boundary conditions, restricting the movement of the base of the heart to impede rigid body motion [Gurev & Lee2011, Kerckhoffs & Neal 2007, Niederer & Plank, 2011]. This constitutes a significant limitation when considering the delicate interaction of the heart with surrounding tissue. As can be observed in dynamic MRI scans, there is no spot within the heart remaining throughout a contraction cycle. Consequently, Dirichlet boundary conditions should not be applied anywhere directly at the heart's surface.

Cardiac motion is constrained by the large vessels and the pericardium which envelops the entire heart. The inner sheet of the pericardium, the pericardium serosum, secretes a liquid which fills the tight space between the epicardium and pericardium. The volume of this space has to remain constant over a cardiac cycle, which, overall, keeps pericardium and epicardium close together. Further, a thin liquid film is always present, thus no-shear forces are transduced, rendering the sliding of the epicardium over the pericardium frictionless. The pericardium elastically adheres to the connective tissue forming the mediastinum, which restricts the motion of the pericardium. The pericardium in turn exerts a restrictive force upon the heart to prevent its dilation [Holt 1970]. This is reflected in the negative pressure inside the epicardial-pericardial gap, which compensates the forces due to myocardial contraction and the restraining forces due to the anchoring with the mediastinum. This restraining effect due to the presence of the pericardium can be accounted for by imposing Neumann boundary conditions over the epicardium, assuming that the time course of pressures within the pericardial gap is known [Kerckhoffs & Omens, 2010]. These physiological boundary conditions are summarized in Figure 13A.

The heart is also anchored to surrounding tissue at the larger vessels attached to the atria. Both atrio-ventricular mechanical interaction and pericardial sliding are considered key mediators of systolic function, as these allow for large displacements of the atrio-ventricular plane. That is, blood is pushed out from the ventricular cavities by the downward motion of the atrio-ventricular plane and, to a much lesser extent, by radial contraction. Capturing these important mechanisms in a model thus requires the explicit inclusion of the atria as well as an explicit addressing of the epicardial-pericardial contact problem [Fritz 2014].

Implementation

As proposed, we implemented alternative methods for enforcing Dirichlet boundary conditions. Unlike in most published studies, the key objective of our implementation is to avoid the mechanical fixing of the basal plane. Such boundary conditions prevent any atrio-ventricular plane displacement, thus changing the dynamics of the outflow tract motion, which is likely to be of importance when considering the outflow of blood during ejection in the computational fluid flow simulations in WP5. A realistic implementation of frictionless boundary conditions imposed by pericardium and mediastinum is beyond the scope of this project. This alone would constitute a research project in its own right, as a mechanical contact problem has to be dealt with, which is challenging to solve. Instead, we opted for implementing two approaches, depending on whether a four chamber heart model or a simpler LV model is being used in a patient simulation. Both approaches offer two distinct advantages over using (bi-)ventricular models with an immobilized base: i) atrioventricular plane displacement is possible; ii) only those locations of the heart or attached vessels are mechanically fixed, which are moving the least during a cardiac cylce, such as the orifices of the large veins, the orificies of the pulmonary veins as well as the open outflow boundaries of the Aorta. The apex of the heart was elastically anchored as well, attempting to keep the heart in its position. Using these boundary conditions, simulations could be performed with satisfactory convergence behavior of the non-linear deformation solver. The application of the boundary conditions is illustrated in Figure 13B and C.

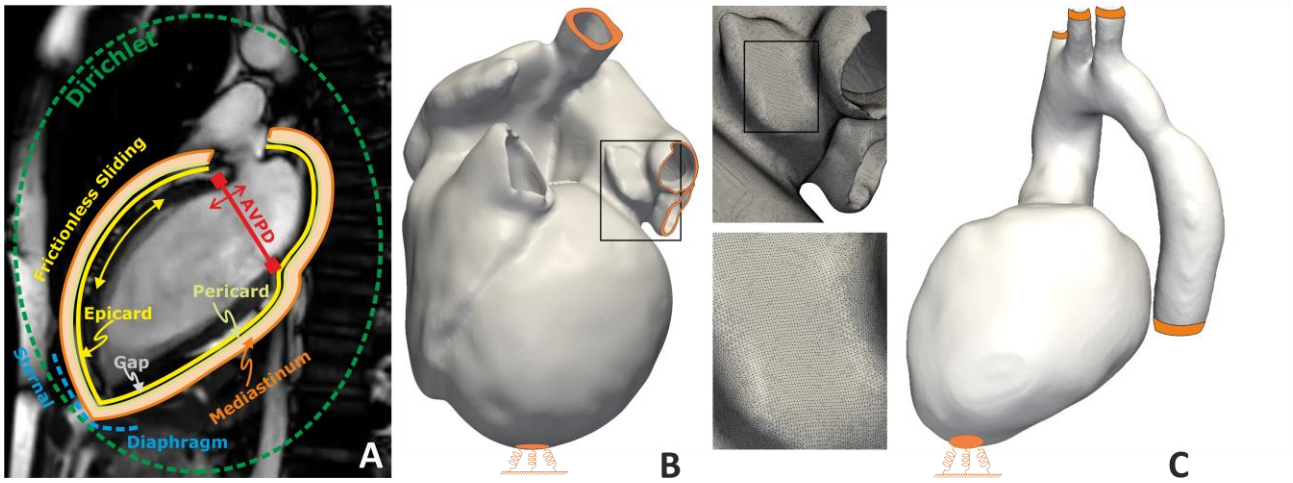

Figure 13 Mechanical boundary conditions. A) In-vivo boundary conditions are complex. The heart slides without friction within the pericardium. The pericardium is loosely anchored within the torso by means of the mediastinum. Dirichlet boundary conditions are only applicable in a certain distance away from the heart. With four chamber (B) and LV models (C), the orificies of the large vessels are kept fixed. In addition, elastic boundary conditions are applied at the apex.

Bibliography

[Aguado-Sierra 2011] Aguado-Sierra, J, A Krishnamurthy, C Villongco, J Chuang, E Howard, MJ Gonzales, J Omens, DE Krummen, S Narayan, RCP Kerckhoffs, and AD McCulloch. Patient-Specific Modeling of Dyssynchronous Heart Failure: A Case Study. Progress in Biophysics and Molecular Biology 107(1):147-55, 2011.

[Constantino 2012] Constantino, J, Y Hu, and NA Trayanova. A computational approach to understanding the cardiac electromechanical activation sequence in the normal and failing heart, with translation to the clinical practice of CRT. Progress in Biophysics and Molecular Biology 110(2-3):372-9, 2012.

[Fritz 2014] Fritz T, Wieners C, Seemann G, Steen H, Doeossel O. Simulation of the contraction of the ventricles in a human heart model including atria and pericardium. Biomech Model Mechanobiol. 13(3):627-41, 2014.

[Gurev 2011] Gurev, V, T Lee, J Constantino, H Arevalo, and NA Trayanova. Models of cardiac electromechanics based on individual hearts imaging data: Image-based electromechanical models of the heart. Biomechanics and Modeling in Mechanobiology 10(3):295-306, 2011.

[Holt 1970] Holt JP. The normal pericardium. Am J Cardiol 26(5):455-465, 1970.

[Hu 2013] Hu, Y, V Gurev, J Constantino, and N Trayanova. Efficient preloading of the ventricles by a properly timed atrial contraction underlies stroke work improvement in the acute response to cardiac resynchronization therapy. Heart Rhythm 10(12):1800-6, 2013.

[Hu 2014] Hu, Y, V Gurev, J Constantino, and N Trayanova. Optimizing cardiac resynchronization therapy to minimize ATP consumption heterogeneity throughout the left ventricle: a simulation analysis using a canine heart failure model. Heart Rhythm 11(6):1063-9, 2014.

[Kerckhoffs & Neal 2007] Kerckhoffs, RCP, ML Neal, Q Gu, JB Bassingthwaighte, JH Omens, and AD McCulloch. Coupling of a 3D Finite Element Model of Cardiac Ventricular Mechanics to Lumped Systems Models of the Systemic and Pulmonic Circulation. Annals of Biomedical Engineering 35(1):1-18, 2007.

[Kerckhoffs 2007] Kerckhoffs, RCP, AD McCulloch, JH Omens, and LJ Mulligan. Effect of Pacing Site and Infarct Location on Regional Mechanics and Global Hemodynamics in a Model Based Study of Heart Failure. In: FIMH 2007, pp. 350-360.

[Kerckhoffs & Omens 2010] Kerckhoffs RCP, Omens JH, McCulloch AD, Mulligan LJ. Ventricular dilation and electrical dyssynchrony synergistically increase regional mechanical nonuniformity but not mechanical dyssynchrony: a computational model. Circ Heart Fail 3(4):528-536, 2010.

[Kerckhoffs 2009] Kerckhoffs, RCP, AD McCulloch, JH Omens, and LJ Mulligan. Effects of biventricular pacing and scar size in a computational model of the failing heart with left bundle branch block. Medical Image Analysis 13(2):362-9, 2009.

[Klotz 2007] Klotz S, ML Dickstein, and D Burkhoff. A computational method of prediction of the end-diastolic pressure-volume relationship by single beat. Nature Protocols 2(9):2152-2158, 2007.

[Krishnamurthy 2013] Krishnamurthy, A, CT Villongco, J Chuang, LR Frank, V Nigam, E Belezzuoli, P Stark, DE Krummen, S Narayan, JH Omens, AD McCulloch, and RCP Kerckhoffs. Patient-Specic Models of Cardiac Biomechanics. Journal of Computational Physics 244:4{21, 2013.

[Marchesseau 2013] Marchesseau, S, H Delingette, M Sermesant, and N Ayache. Fast parameter calibration of a cardiac electromechanical model from medical images based on the unscented transform. Biomechanics and Modeling in Mechanobiology 12(4):815{31, 2013.

[Niederer & Lamata 2012] Niederer, SA, P Lamata, G Plank, P Chinchapatnam, M Ginks, KS Rhode, CA Rinaldi, R Razavi, and NP Smith. Analyses of the Redistribution of Work following Cardiac Resynchronisation Therapy in a Patient Specific Model. PloS One 7(8):e43504, 2012.

[Niederer & Plank 2011] Niederer SA, Plank G, Chinchapatnam P, Ginks M, Lamata P, Rhode KS, Rinaldi CA, Razavi R, Smith NP. Length-dependent tension in the failing heart and the efficacy of cardiac resynchronization therapy. Cardiovascular Research 89(2):336-343, 2011.

[Niederer 2012] Niederer, SA, AK Shetty, G Plank, J Bostock, R Razavi, NP Smith, and CA Rinaldi. Biophysical Modeling to Simulate the Response to Multisite Left Ventricular Stimulation Using a Quadripolar Pacing Lead. Pacing and Clinical Electrophysiology 35(2):204{214, 2012.

[Niederer 2011] Niederer, SA, G Plank, P Chinchapatnam, M Ginks, P Lamata, KS Rhode, CA Rinaldi, R Razavi, and NP Smith. Length-dependent tension in the failing heart and the efficacy of cardiac resynchronization therapy. Cardiovascular Research 89(2):336{43, 2011.

[Rajagopol 2008] Rajagopal V, Nash M, Highnam R, Nielsen P. The Breast Biomechanics Reference State for Multi-modal Image Analysis. Digital Mammography, 385-392, 2008.

[Sermesant 2012] Sermesant, M, R Chabiniok, P Chinchapatnam, T Mansi, F Billet, P Moireau, JM Peyrat, K Wong, J Relan, K Rhode, M Ginks, P Lambiase, H Delingette, M Sorine, CA Rinaldi, D Chapelle, R Razavi, and N Ayache. Patient-specific electromechanical models of the heart for the prediction of pacing acute effects in CRT: A preliminary clinical validation. Medical Image Analysis 16(1):201-15, 2012.

[Stergiopulos 1999] Stergiopulos, N, BE Westerhof, and N Westerhof. Total arterial inertance as the fourth element of the windkessel model. The American Journal of Physiology 276(1Pt 2):H81{8, 1999.

[Sugiura 2012] Sugiura, S, T Washio, A Hatano, J Okada, H Watanabe, and T Hisada. Multi-scale simulations of cardiac electrophysiology and mechanics using the University of Tokyo heart simulator. Progress in Biophysics and Molecular Biology 110(2-3):380{9, 2012.

[Westerhof 1971] Westerhof, N., G. Elzinga, and P. Sipkema. An artificial arterial system for pumping hearts. J. Appl. Physiol. 31: 776– 781, 1971.